

Journal of Mechanics of Materials and Structures

**A PERFECTLY MATCHED LAYER
FOR PERIDYNAMICS IN TWO DIMENSIONS**

Raymond A. Wildman and George A. Gazonas

Volume 7, No. 8-9

October 2012



A PERFECTLY MATCHED LAYER FOR PERIDYNAMICS IN TWO DIMENSIONS

RAYMOND A. WILDMAN AND GEORGE A. GAZONAS

A perfectly matched layer (PML) absorbing boundary is formulated for and numerically applied to peridynamics in two dimensions. Peridynamics is a nonlocal method, derived to be insensitive to discontinuities, more easily simulating fracture. A PML is an absorbing boundary layer, which decays impinging waves exponentially without introducing reflections at the boundary between the computational region and the absorbing layer. Here, we use state-based peridynamics as PMLs are essentially anisotropic absorbing materials, therefore requiring arbitrary material parameters. State-based peridynamics is also more convenient for auxiliary field formulations, facilitating the implementation of the PML. Results show the efficacy of the approach.

1. Introduction

Originally introduced in [Silling 2000], peridynamics is a nonlocal formulation of elastodynamics, which can more easily incorporate discontinuities such as cracks and damage. Derivatives of field variables in the classical continuum model are replaced by integrals over a small neighborhood of microelastic kernels that replace standard constitutive relations. In its discretized form, an elastic solid is treated as a collection of particles or nodes, each connected to its neighbors by breakable bonds. Bond breakage can be defined to occur when a bond is stretched past some predetermined limit. After a bond is broken, any supported force transfers to the remaining bonds, increasing their supported load, and encouraging more breakage. Eventually, this process autonomously leads to cracking and failure. The end result is a method capable of predicting crack growth in brittle elastic materials [Gerstle et al. 2005; Silling and Askari 2005; Emmrich and Weckner 2006; Demmie and Silling 2007; Kilic et al. 2009; Ha and Bobaru 2010].

Over the last decade, peridynamics has been extended past its original formulation. First, the numerical method originally outlined in [Silling and Askari 2005] has been extended to include adaptive refinement [Bobaru et al. 2009], replaced with different quadrature rules [Emmrich and Weckner 2007], and implemented in a parallel, molecular dynamics code [Parks et al. 2008]. In addition, it has been extended to different material types including viscoplastic [Foster et al. 2010], micropolar [Gerstle et al. 2011], and nanofiber networks [Bobaru 2007]. It has also been applied to different fields such as heat conduction [Bobaru and Duangpanya 2010] and electromigration [Gerstle et al. 2008]. Aside from practical applications, the mathematics behind the approach have been studied: Weckner et al. [2009] derived a Green's function for the peridynamic equation and Weckner and Abeyaratne [2005] discussed dispersion relations for various kernels. Most importantly for this work, state-based peridynamics was introduced,

Keywords: peridynamics, perfectly matched layer, absorbing boundary.

allowing for more flexible constitutive relations [Silling et al. 2007]. As will become clear later, state-based peridynamics allows for an auxiliary field formulation, which is necessary for the implementation of a perfectly matched layer (PML).

While most peridynamics work has focused on simulating problems with free or fixed boundary conditions, there are applications in which the simulation of an infinite medium may be useful, such as wave or crack propagation in a half-space. Absorbing boundary conditions are a way of simulating an infinite medium by absorbing any impinging waves at the computational boundaries so they do not reflect back into the simulation. A PML is such an absorbing boundary, and was originally introduced for electromagnetic simulations [Berenger 1994; Chew and Weedon 1994]. PMLs differ from traditional absorbing boundary conditions in that they are an absorbing layer, placed between the computational region of interest and the truncation of the grid or mesh. They can also be thought of as an anisotropic absorbing material, which is why the flexibility of a state-based peridynamics is necessary.

PMLs have two important qualities: First, waves in a PML decay exponentially, and second, in their analytic form, no waves reflect at the interface of a PML and the computational region. These properties make them ideal for simulating wave propagation in infinite, unbounded regions. Since their introduction, PMLs have been extended to many different types of media [Uno et al. 1997; Teixeira and Chew 1998; Dong et al. 2004], different numerical methods [Pissoort and Olyslager 2003; Pissoort et al. 2005; Alles and van Dongen 2009], and different fields [Chew and Liu 1996; Liu and Tao 1997; Festa and Nielsen 2003].

This paper implements a peridynamic formulation of elastodynamics in two dimensions and terminates the boundary with a PML. As is discussed, the use of a PML is facilitated with an auxiliary field formulation, derived from state-based peridynamics, and the peridynamic equation is broken into five coupled equations. A PML was applied to one-dimensional peridynamics in [Wildman and Gazonas 2011], which used the results of [Du et al. 2012] to formulate an auxiliary field equation. This approach required a matrix representation of the auxiliary field, which may be memory prohibitive in higher dimensions.

The remainder of the paper is organized as follows: Section 2 discusses the formulation of peridynamics, PMLs, and their numerical implementation; Section 3 gives some results; and Section 4 summarizes the report and details future work.

2. Formulation

In this section, a PML is formulated for state-based two-dimensional peridynamics. First, in Section 2A, a linear elastic, state-based peridynamics formulation will be reviewed. Next, Section 2B reviews the formulation of a PML. Section 2C then applies the PML to state-based peridynamics, and finally Section 2D discusses a discretization of the formulation using the standard node-based peridynamics method.

2A. Two-dimensional, state-based peridynamics. The continuum equation of motion in an elastic solid can be stated as

$$\rho \frac{\partial^2}{\partial t^2} \mathbf{u} = \nabla \cdot \bar{\boldsymbol{\sigma}} + \mathbf{b}, \quad (2-1)$$

where (in two dimensions) $\rho(\mathbf{x})$ [kg/m²] is the density, $\mathbf{u}(\mathbf{x}, t)$ [m] is the displacement, $\bar{\boldsymbol{\sigma}}(\mathbf{x}, t)$ [N/m] is the stress tensor, and $\mathbf{b}(\mathbf{x})$ [N/m²] is a body force [Malvern 1969]. (Throughout, boldface type denotes a vector and a boldface variable with an overbar denotes a tensor.) Equation (2-1) is a local formulation

because the divergence of the stress (and gradient of the displacement implied in its definition) represents a local operation on a variable. In other words, the action of $\nabla \cdot \bar{\sigma}$ only depends on $\bar{\sigma}$ at a single spatial point. In problems involving discontinuities, such as cracks, the divergence at such discontinuities is not well defined, leading to numerical implementation problems. Peridynamics proposes replacing $\nabla \cdot \bar{\sigma}$ with a nonlocal operation that nonetheless also represents a force

$$\rho \frac{\partial^2}{\partial t^2} \mathbf{u} = \int_{\mathcal{H}_x} \mathbf{f}(\mathbf{u}' - \mathbf{u}, \mathbf{x}' - \mathbf{x}) dV_{x'} + \mathbf{b}, \tag{2-2}$$

where $\mathbf{f}(\mathbf{x}' - \mathbf{x}, \mathbf{u}' - \mathbf{u})$ [N/m⁴] represents a micromodulus force function (or kernel) that defines a force between two points and \mathcal{H}_x represents a horizon or maximum distance over which two points can influence each other [Silling 2000]. The micromodulus function becomes the constitutive response in the formulation, replacing Hooke’s law in the continuum case. In its original form, the micromodulus function was developed as a simple elastic response following

$$\mathbf{f}(\boldsymbol{\eta}, \boldsymbol{\xi}) = c \frac{\boldsymbol{\xi} + \boldsymbol{\eta}}{|\boldsymbol{\xi} + \boldsymbol{\eta}|} \frac{|\boldsymbol{\xi} + \boldsymbol{\eta}| - |\boldsymbol{\eta}|}{|\boldsymbol{\eta}|} H(\delta - |\boldsymbol{\xi}|), \tag{2-3}$$

where c is some constant, $H(\cdot)$ is the Heaviside step function, and δ is the radius of the horizon region, which defines \mathcal{H}_x [Silling 2000]. Note that in contrast to [Silling 2000], for simplicity there is no history-dependent failure term in (2-3). Equation (2-3) is isotropic, though not strictly linear in terms of \mathbf{u} . Linearizing (2-3) gives

$$\mathbf{f}(\boldsymbol{\eta}, \boldsymbol{\xi}) = \bar{\mathbf{C}}(\boldsymbol{\xi})\boldsymbol{\eta}, \quad \bar{\mathbf{C}}(\boldsymbol{\xi}) = C(\boldsymbol{\xi}) \frac{\boldsymbol{\xi} \otimes \boldsymbol{\xi}}{|\boldsymbol{\xi}|^3}, \quad C(|\boldsymbol{\xi}|) = cH(\delta - |\boldsymbol{\xi}|), \tag{2-4}$$

where \otimes denotes an outer product [Silling 2000]. The function $C(|\boldsymbol{\xi}|)$ is the kernel function, typically taken to be a Heaviside function. Here, we will also use a Gaussian kernel function, which tends to give smoother results with less apparent ringing in the solution. A Gaussian kernel is defined as

$$C_{\text{Gauss}}(|\boldsymbol{\xi}|) = ce^{-(|\boldsymbol{\xi}|/\delta)^2}. \tag{2-5}$$

For the Gaussian kernel, the horizon δ does not delineate a strict bond family as the Heaviside function, but describes the decay of the kernel. To determine the bond family, \mathcal{H}_x , a small, arbitrary value can be chosen as a cutoff for the kernel. Note that the cutoff has a large impact on the efficiency of the method: too small a cutoff and a large number of bonds must be included in each calculation. Throughout, we set the cutoff to 10^{-6} .

A PML application requires an auxiliary field formulation, as it is essentially an anisotropic absorbing material, if a nonphysical one. Consequently, a state-based peridynamic formulation [Silling et al. 2007] is necessary to implement the required constitutive relations in the absorber. State-based peridynamics uses a family of bonds to determine a given force rather than a single bond independently. This more general approach allows for inelastic behavior and more general elastic behavior, and is governed by

$$\rho \frac{\partial^2}{\partial t^2} \mathbf{u} = \int_{\mathcal{H}_x} (\bar{\mathbf{T}}[\mathbf{x}, t](\mathbf{x}' - \mathbf{x}) - \bar{\mathbf{T}}[\mathbf{x}', t](\mathbf{x} - \mathbf{x}')) dV_{x'} + \mathbf{b}, \tag{2-6}$$

where $\bar{\mathbf{T}}[\mathbf{x}, t](\mathbf{x}' - \mathbf{x})$ is a peridynamic vector state, with the parameters in the square brackets indicating variables that act as arguments to any functions referenced in the vector state and the variables in the

angle brackets acting as arguments to the vector state itself. In the state-based formulation of [Foster et al. 2010], the deformation gradient, given by

$$\bar{\mathbf{F}} = \bar{\mathbf{I}} + \mathbf{u}\nabla, \quad (2-7)$$

can be approximated as a vector state as

$$\bar{\mathbf{F}}[\mathbf{x}, t] = \left[\int_{\mathcal{H}_x} C(|\xi|) (\mathbf{Y}[\mathbf{x}, t](\xi) \otimes \xi) dV_{x'} \right] \bar{\mathbf{K}}^{-1}, \quad (2-8)$$

where $\xi = \mathbf{x}' - \mathbf{x}$, $\bar{\mathbf{K}}$ is a shape tensor given by

$$\bar{\mathbf{K}}[\mathbf{x}, t] = \int_{\mathcal{H}_x} C(|\xi|) (\xi \otimes \xi) dV_{x'}, \quad (2-9)$$

and \mathbf{Y} is a deformation vector state given by

$$\mathbf{Y}[\mathbf{x}, t](\xi) = \boldsymbol{\eta} + \xi, \quad (2-10)$$

with $\boldsymbol{\eta} = \mathbf{u}[\mathbf{x}', t] - \mathbf{u}[\mathbf{x}, t]$ [Foster et al. 2010].

The deformation gradient can now be substituted into Hooke's law and strain-displacement relations, giving a stress term $\bar{\boldsymbol{\sigma}}$ in terms of \mathbf{u} in plane strain

$$\rho \frac{\partial^2 \mathbf{u}}{\partial t^2} = \nabla \cdot \bar{\boldsymbol{\sigma}} = \nabla \cdot (\bar{\mathbf{c}} : \bar{\boldsymbol{\epsilon}}), \quad (2-11)$$

where

$$\bar{\boldsymbol{\epsilon}}[\mathbf{x}, t] = \frac{1}{2} (\nabla \mathbf{u} + \mathbf{u} \nabla) = \frac{1}{2} (\bar{\mathbf{F}}[\mathbf{x}, t] + \bar{\mathbf{F}}[\mathbf{x}, t]^T - 2\bar{\mathbf{I}}), \quad (2-12)$$

$$\bar{\mathbf{c}} = \frac{E}{(1+\nu)(1-2\nu)} \begin{bmatrix} 1-\nu & \nu & 0 \\ \nu & 1-\nu & 0 \\ 0 & 0 & 1-2\nu \end{bmatrix} = \begin{bmatrix} \lambda+2\mu & \lambda & 0 \\ \lambda & \lambda+2\mu & 0 \\ 0 & 0 & 2\mu \end{bmatrix}, \quad (2-13)$$

E is the Young's modulus, ν is the Poisson's ratio, and λ and μ are the Lamé parameters. Ultimately, the peridynamic vector state \mathbf{T} for plane strain elasticity is given by

$$\bar{\mathbf{T}}[\mathbf{x}, t](\xi) = C(|\xi|) \bar{\boldsymbol{\sigma}}[\mathbf{x}, t] \bar{\mathbf{K}}^{-1} \xi. \quad (2-14)$$

2B. Perfectly matched layer. The first step in formulating a PML is to construct an analytic continuation to the complex plane

$$\hat{x} = x + ig(x), \quad (2-15)$$

where $g(x)$ is a given function describing the deformation [Johnson 2010]. This mapping has the effect of transforming traveling waves of the form e^{ikx} , where $k = \omega/c$ is the wave number, into evanescent waves of the form $e^{ikx} e^{-kg(x)}$, thus attenuating such waves in the PML region.

Substituting \hat{x} into the above equations would yield a viable method, though one that requires complex coordinates. A simpler solution is to change variables back to the real part x , which requires a relation

for the differential quantities, given as

$$\partial \hat{x} = \left[1 + i \frac{d}{dx} g \right] \partial x; \tag{2-16}$$

partial differential quantities are used, as this is used as a substitution for the above equations involving functions of both x and t [Johnson 2010]. A convenient choice for $g(x)$ is

$$\frac{d}{dx} g(x) = \frac{\phi(x)}{\omega}, \tag{2-17}$$

because the $1/\omega$ factor creates a frequency-independent attenuation rate in dispersionless materials [Johnson 2010]. (Peridynamic formulations are not dispersionless, as discussed in [Weckner and Abeyaratne 2005], though this standard choice is used for simplicity.) Finally, the substitution that must be made for any spatial derivative can be written

$$\frac{\partial}{\partial x} \rightarrow \frac{1}{1 + i\phi(x)/\omega} \frac{\partial}{\partial x}. \tag{2-18}$$

Before applying a PML directly to the peridynamic equation, (2-1) will be treated so that the PML application to peridynamics will be clear. It is convenient to convert (2-1) to the Laplace domain, assuming e^{-st} time dependence, giving

$$\rho s^2 \tilde{\mathbf{u}} = \nabla \cdot \tilde{\boldsymbol{\sigma}}, \tag{2-19}$$

where the Laplace transform of a variable is indicated by $\mathcal{L}\{f\} = \tilde{f}$. Next, we express the wave equation as two coupled first-order partial differential equations, the first in $\tilde{\mathbf{u}}$ and the second in $s\tilde{\boldsymbol{\psi}} = \tilde{\boldsymbol{\sigma}}$:

$$\rho s \tilde{\mathbf{u}} = \nabla \cdot \tilde{\boldsymbol{\psi}}, \quad s \tilde{\boldsymbol{\psi}} = \tilde{\mathbf{c}} : \tilde{\boldsymbol{\epsilon}}. \tag{2-20}$$

Expanding (2-20) into components gives five coupled equations:

$$\begin{aligned} \rho s \tilde{u}_x &= \frac{\partial}{\partial x} \tilde{\psi}_x + \frac{\partial}{\partial y} \tilde{\psi}_\tau, & \rho s \tilde{u}_y &= \frac{\partial}{\partial x} \tilde{\psi}_\tau + \frac{\partial}{\partial y} \tilde{\psi}_y, \\ s \tilde{\psi}_x &= (\lambda + 2\mu) \frac{\partial}{\partial x} \tilde{u}_x + \lambda \frac{\partial}{\partial y} \tilde{u}_y, & s \tilde{\psi}_y &= \lambda \frac{\partial}{\partial x} \tilde{u}_x + (\lambda + 2\mu) \frac{\partial}{\partial y} \tilde{u}_y, & s \tilde{\psi}_\tau &= \mu \left(\frac{\partial}{\partial y} \tilde{u}_x + \frac{\partial}{\partial x} \tilde{u}_y \right). \end{aligned} \tag{2-21}$$

Here, we will make the substitution given in (2-18) for all spatial derivatives, written as

$$\frac{\partial}{\partial x} \rightarrow \frac{s}{s + \phi(x)} \frac{\partial}{\partial x} \tag{2-22}$$

in the Laplace domain, and later define ϕ_x and ϕ_y in the desired absorbing boundary locations. Using (2-21)₁ as an example, we get

$$\begin{aligned} \rho s \tilde{u}_x &= \frac{s}{s + \phi_x} \frac{\partial}{\partial x} \tilde{\psi}_x + \frac{s}{s + \phi_y} \frac{\partial}{\partial y} \tilde{\psi}_\tau \\ \implies \rho (s + \phi_x)(s + \phi_y) \tilde{u}_x &= (s + \phi_y) \frac{\partial}{\partial x} \tilde{\psi}_x + (s + \phi_x) \frac{\partial}{\partial y} \tilde{\psi}_\tau. \end{aligned} \tag{2-23}$$

The remaining components of (2-21) can be expanded in a similar way.

Wherever $\phi > 0$, \mathbf{u} and $\boldsymbol{\sigma}$ will exponentially decay. Before discretization, any change in ϕ will not result in any reflections, so the region of interest would have $\phi = 0$, and the PML region could have a

discontinuity in applying ϕ . In practice, however, numerical reflections can result from discontinuous material parameters after discretization, so it is better to use a smooth transition for ϕ . Here, we divide the PML region into two parts, one in which ϕ is a constant value, and the other in which ϕ ramps up to that constant value following a Gaussian distribution. An example is shown in Figure 1, with the constant region set to 0.1 m and the Gaussian region 0.2 m. The variance of the distribution is set so that the minimum value in the Gaussian region is 10^{-6} .

2C. Auxiliary field formulation and PML application. Peridynamics is not typically stated in terms of Cartesian components as in (2-24), but we can expand the state-based formulation into components and match terms to (2-24). Following this approach yields a viable method for performing PML substitutions.

First, the state-based peridynamic equations (2-6)–(2-14) can be written explicitly as

$$\begin{aligned}
\rho s \tilde{u}_x[\mathbf{x}, s] &= \int_{\mathcal{H}_x} C(|\xi|) [(\tilde{\psi}_x[\mathbf{x}, s] k_{xx}^{\text{inv}} + \tilde{\psi}_\tau[\mathbf{x}, s] k_{yy}^{\text{inv}}) \xi_x + (\tilde{\psi}_x[\mathbf{x}', s] k_{xx}^{\text{inv}} + \tilde{\psi}_\tau[\mathbf{x}', s] k_{yy}^{\text{inv}}) \xi_x] dV_{x'} \\
&\quad + \int_{\mathcal{H}_x} C(|\xi|) [(\tilde{\psi}_x[\mathbf{x}, s] k_{xy}^{\text{inv}} + \tilde{\psi}_\tau[\mathbf{x}, s] k_{yy}^{\text{inv}}) \xi_y + (\tilde{\psi}_x[\mathbf{x}', s] k_{xy}^{\text{inv}} + \tilde{\psi}_\tau[\mathbf{x}', s] k_{yy}^{\text{inv}}) \xi_y] dV_{x'}, \\
\rho s \tilde{u}_y[\mathbf{x}, s] &= \int_{\mathcal{H}_x} C(|\xi|) [(\tilde{\psi}_\tau[\mathbf{x}, s] k_{xx}^{\text{inv}} + \tilde{\psi}_y[\mathbf{x}, s] k_{yx}^{\text{inv}}) \xi_x + (\tilde{\psi}_\tau[\mathbf{x}', s] k_{xx}^{\text{inv}} + \tilde{\psi}_y[\mathbf{x}', s] k_{yx}^{\text{inv}}) \xi_x] dV_{x'} \\
&\quad + \int_{\mathcal{H}_x} C(|\xi|) [(\tilde{\psi}_\tau[\mathbf{x}, s] k_{xy}^{\text{inv}} + \tilde{\psi}_y[\mathbf{x}, s] k_{yy}^{\text{inv}}) \xi_y + (\tilde{\psi}_\tau[\mathbf{x}', s] k_{xy}^{\text{inv}} + \tilde{\psi}_y[\mathbf{x}', s] k_{yy}^{\text{inv}}) \xi_y] dV_{x'}, \\
s \tilde{\psi}_x[\mathbf{x}, s] &= (\lambda + 2\mu) \left[\int_{\mathcal{H}_x} C(|\xi|) (\tilde{Y}_x[\mathbf{x}, s] \xi_x k_{xx}^{\text{inv}} + \tilde{Y}_x[\mathbf{x}, s] \xi_y k_{yx}^{\text{inv}}) dV_{x'} - 1 \right] \\
&\quad + \lambda \left[\int_{\mathcal{H}_x} C(|\xi|) (\tilde{Y}_y[\mathbf{x}, s] \xi_x k_{xy}^{\text{inv}} + \tilde{Y}_y[\mathbf{x}, s] \xi_y k_{yy}^{\text{inv}}) dV_{x'} - 1 \right], \\
s \tilde{\psi}_y[\mathbf{x}, s] &= \lambda \left[\int_{\mathcal{H}_x} C(|\xi|) (\tilde{Y}_x[\mathbf{x}, s] \xi_x k_{xx}^{\text{inv}} + \tilde{Y}_x[\mathbf{x}, s] \xi_y k_{yx}^{\text{inv}}) dV_{x'} - 1 \right] \\
&\quad + (\lambda + 2\mu) \left[\int_{\mathcal{H}_x} C(|\xi|) (\tilde{Y}_y[\mathbf{x}, s] \xi_x k_{xy}^{\text{inv}} + \tilde{Y}_y[\mathbf{x}, s] \xi_y k_{yy}^{\text{inv}}) dV_{x'} - 1 \right], \\
s \tilde{\psi}_\tau[\mathbf{x}, s] &= \mu \int_{\mathcal{H}_x} C(|\xi|) (\tilde{Y}_x[\mathbf{x}, s] \xi_x k_{xy}^{\text{inv}} + \tilde{Y}_x[\mathbf{x}, s] \xi_y k_{yy}^{\text{inv}}) dV_{x'} \\
&\quad + \mu \int_{\mathcal{H}_x} C(|\xi|) (\tilde{Y}_y[\mathbf{x}, s] \xi_x k_{xx}^{\text{inv}} + \tilde{Y}_y[\mathbf{x}, s] \xi_y k_{yx}^{\text{inv}}) dV_{x'}, \quad (2-24)
\end{aligned}$$

where

$$\bar{\mathbf{K}}^{-1} = \begin{bmatrix} k_{xx}^{\text{inv}} & k_{xy}^{\text{inv}} \\ k_{yx}^{\text{inv}} & k_{yy}^{\text{inv}} \end{bmatrix}. \quad (2-25)$$

Though no derivatives appear in (2-24), the correspondence of each term to those in (2-21) is apparent — with partial derivatives following the component of ξ — and the PML substitutions can be made. For

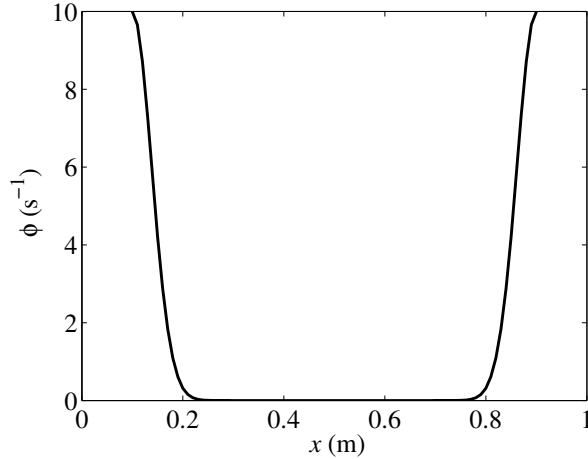


Figure 1. An example of a PML across one dimension using a Gaussian ramp.

example, the first equation in (2-24) can be rewritten as

$$\begin{aligned}
 \rho(s + \phi_x)(s + \phi_y)\tilde{u}_x = & (s + \phi_y) \int_{\mathcal{H}_x} C(|\xi|)(\tilde{\psi}_x[\mathbf{x}, s]k_{xx}^{inv} + \tilde{\psi}_{xy}[\mathbf{x}, s]k_{yx}^{inv})\xi_x dV_{x'} \\
 & + (s + \phi_y) \int_{\mathcal{H}_x} C(|\xi|)(\tilde{\psi}_x[\mathbf{x}', s]k_{xx}'^{inv} + \tilde{\psi}_{xy}[\mathbf{x}', s]k_{yx}'^{inv})\xi_x dV_{x'} \\
 & + (s + \phi_x) \int_{\mathcal{H}_x} C(|\xi|)(\tilde{\psi}_x[\mathbf{x}, s]k_{xy}^{inv} + \tilde{\psi}_\tau[\mathbf{x}, s]k_{yy}^{inv})\xi_y dV_{x'} \\
 & + (s + \phi_x) \int_{\mathcal{H}_x} C(|\xi|)(\tilde{\psi}_x[\mathbf{x}', s]k_{xy}'^{inv} + \tilde{\psi}_\tau[\mathbf{x}', s]k_{yy}'^{inv})\xi_y dV_{x'}, \quad (2-26)
 \end{aligned}$$

with the remaining equations following similarly.

2D. Discretization. For the temporal discretization, forward Euler will be used to simplify the presentation and implementation. Higher-order temporal discretizations can be used, though they lead to more terms in what follows. The Laplace domain was used throughout to facilitate the temporal discretization of the final equations. Because differentiation in the Laplace domain is represented by s , approximations to s can be directly substituted in terms of the z -transform. This technique is used in the design of digital filters, where it is known as “filter design by approximation of derivatives” or “the bilinear transformation” [Proakis and Manolakis 1996], and in integral equation methods where it is known as “convolution quadrature” [Lubich 1988a; 1988b], or “finite difference delay modeling” [Wang et al. 2008]. A forward Euler approximation can be stated as the substitution

$$s \rightarrow \frac{z-1}{\Delta t}, \quad (2-27)$$

where z is the z -transform¹ variable representing a unit advance and Δt is the time step size. Substitution

¹The z -transform is defined here as $X(z) = Z\{x[n]\} = \sum_{n=0}^{\infty} x[n]z^{-n}$ for causal signals.

into (2-26) gives

$$\begin{aligned}
\rho(z-1+\Delta t\phi_x)(z-1+\Delta t\phi_y)U_x &= (z-1+\Delta t\phi_y) \int_{\mathcal{H}_x} C(|\xi|)(\Psi_x[\mathbf{x}, z]k_{xx}^{\text{inv}} + \Psi_\tau[\mathbf{x}, z]k_{yx}^{\text{inv}}) \xi_x dV_{\mathbf{x}'} \\
&+ (z-1+\Delta t\phi_y) \int_{\mathcal{H}_x} C(|\xi|)(\Psi_x[\mathbf{x}', z]k_{xx}^{\text{inv}} + \Psi_\tau[\mathbf{x}', z]k_{yx}^{\text{inv}}) \xi_x dV_{\mathbf{x}'} \\
&+ (z-1+\Delta t\phi_x) \int_{\mathcal{H}_x} C(|\xi|)(\Psi_x[\mathbf{x}, z]k_{xy}^{\text{inv}} + \Psi_\tau[\mathbf{x}, z]k_{yy}^{\text{inv}}) \xi_y dV_{\mathbf{x}'} \\
&+ (z-1+\Delta t\phi_x) \int_{\mathcal{H}_x} C(|\xi|)(\Psi_x[\mathbf{x}', z]k_{xy}^{\text{inv}} + \Psi_\tau[\mathbf{x}', z]k_{yy}^{\text{inv}}) \xi_y dV_{\mathbf{x}'}, \quad (2-28)
\end{aligned}$$

where capital letters indicate the z -transform of a variable. Expanding the quadratic term on the left-hand side gives

$$\begin{aligned}
(z-1+\Delta t\phi_x)(z-1+\Delta t\phi_y) &= \Delta t^2\phi_x\phi_y + \Delta t\phi_xz - \Delta t\phi_x + \Delta t\phi_yz + z^2 - z - \Delta t\phi_y - z + 1 \\
&= z^2 + (\Delta t\phi_x + \Delta t\phi_y - 2)z + \Delta t^2\phi_x\phi_y - \Delta t\phi_x - \Delta t\phi_y + 1. \quad (2-29)
\end{aligned}$$

Multiplying by z^{-2} and rearranging gives an update equation in terms of z , which can be converted to a time-stepping method via the inverse z -transform² (assuming vanishing initial conditions and an appropriate region of convergence) as

$$\begin{aligned}
u_x[\mathbf{x}, l] &= -(\gamma_x + \gamma_y)u_x[\mathbf{x}, l-1] - \gamma_x\gamma_y u_x[\mathbf{x}, l-2] \\
&+ \frac{\Delta t}{\rho} \int_{\mathcal{H}_x} C(|\xi|)(\psi_x[\mathbf{x}, l-1]k_{xx}^{\text{inv}} + \psi_\tau[\mathbf{x}, l-1]k_{yx}^{\text{inv}}) \xi_x dV_{\mathbf{x}'} \\
&+ \frac{\Delta t}{\rho} \int_{\mathcal{H}_x} C(|\xi|)(\psi_x[\mathbf{x}', l-1]k_{xx}^{\text{inv}} + \psi_\tau[\mathbf{x}', l-1]k_{yx}^{\text{inv}}) \xi_x dV_{\mathbf{x}'} \\
&+ \frac{\Delta t}{\rho} \gamma_y \int_{\mathcal{H}_x} C(|\xi|)(\psi_x[\mathbf{x}, l-2]k_{xx}^{\text{inv}} + \psi_\tau[\mathbf{x}, l-2]k_{yx}^{\text{inv}}) \xi_x dV_{\mathbf{x}'} \\
&+ \frac{\Delta t}{\rho} \gamma_y \int_{\mathcal{H}_x} C(|\xi|)(\psi_x[\mathbf{x}', l-2]k_{xx}^{\text{inv}} + \psi_\tau[\mathbf{x}', l-2]k_{yx}^{\text{inv}}) \xi_x dV_{\mathbf{x}'} \\
&+ \frac{\Delta t}{\rho} \int_{\mathcal{H}_x} C(|\xi|)(\psi_x[\mathbf{x}, l-1]k_{xy}^{\text{inv}} + \psi_\tau[\mathbf{x}, l-1]k_{yy}^{\text{inv}}) \xi_y dV_{\mathbf{x}'} \\
&+ \frac{\Delta t}{\rho} \int_{\mathcal{H}_x} C(|\xi|)(\psi_x[\mathbf{x}', l-1]k_{xy}^{\text{inv}} + \psi_\tau[\mathbf{x}', l-1]k_{yy}^{\text{inv}}) \xi_y dV_{\mathbf{x}'} \\
&+ \frac{\Delta t}{\rho} \gamma_x \int_{\mathcal{H}_x} C(|\xi|)(\psi_x[\mathbf{x}, l-2]k_{xy}^{\text{inv}} + \psi_\tau[\mathbf{x}, l-2]k_{yy}^{\text{inv}}) \xi_y dV_{\mathbf{x}'} \\
&+ \frac{\Delta t}{\rho} \gamma_x \int_{\mathcal{H}_x} C(|\xi|)(\psi_x[\mathbf{x}', l-2]k_{xy}^{\text{inv}} + \psi_\tau[\mathbf{x}', l-2]k_{yy}^{\text{inv}}) \xi_y dV_{\mathbf{x}'}, \quad (2-30)
\end{aligned}$$

²The only necessary property is the delay: $x[n-k] \leftrightarrow z^{-k}X(z)$

where l is the time step number, $\gamma_x = \Delta t \phi_x - 1$, and $\gamma_y = \Delta t \phi_y - 1$. A stress component update equation becomes, for example,

$$\begin{aligned} \psi_x[\mathbf{x}, l] = & -(\gamma_x + \gamma_y)\psi_x[\mathbf{x}, l-1] - \gamma_x\gamma_y\psi_x[\mathbf{x}, l-2] \\ & + \Delta t(\lambda + 2\mu) \left[\int_{\mathcal{H}_x} C(|\xi|)(Y_x[\mathbf{x}, l-1]\xi_x k_{xx}^{\text{inv}} + Y_x[\mathbf{x}, l-1]\xi_y k_{yx}^{\text{inv}}) dV_{\mathbf{x}'} - 1 \right] \\ & + \Delta t\gamma_y(\lambda + 2\mu) \left[\int_{\mathcal{H}_x} C(|\xi|)(Y_x[\mathbf{x}, l-2]\xi_x k_{xx}^{\text{inv}} + Y_x[\mathbf{x}, l-2]\xi_y k_{yx}^{\text{inv}}) dV_{\mathbf{x}'} - 1 \right] \\ & + \Delta t\lambda \left[\int_{\mathcal{H}_x} C(|\xi|)(Y_y[\mathbf{x}, l-1]\xi_x k_{xy}^{\text{inv}} + Y_y[\mathbf{x}, l-1]\xi_y k_{yy}^{\text{inv}}) dV_{\mathbf{x}'} - 1 \right] \\ & + \Delta t\lambda\gamma_x \left[\int_{\mathcal{H}_x} C(|\xi|)(Y_y[\mathbf{x}, l-2]\xi_x k_{xy}^{\text{inv}} + Y_y[\mathbf{x}, l-2]\xi_y k_{yy}^{\text{inv}}) dV_{\mathbf{x}'} - 1 \right]. \end{aligned} \quad (2-31)$$

Finally, (2-30) can be discretized spatially using a simple one-point integration and point match testing, giving, for the x -component of displacement,

$$\begin{aligned} u_x[\mathbf{x}_i, l] = & -(\gamma_x + \gamma_y)u_x[\mathbf{x}_i, l-1] - \gamma_x\gamma_y u_x[\mathbf{x}_i, l-2] \\ & + \frac{\Delta t}{\rho} \sum_{j=1}^{N_i} C(|\xi_{ij}|)(\psi_x[\mathbf{x}_i, l-1]k_{i,xx}^{\text{inv}} + \psi_\tau[\mathbf{x}_i, l-1]k_{i,yx}^{\text{inv}})\xi_x V_j \\ & + \frac{\Delta t}{\rho} \sum_{j=1}^{N_i} C(|\xi_{ij}|)(\psi_x[\mathbf{x}_j, l-1]k_{j,xx}^{\text{inv}} + \psi_\tau[\mathbf{x}_j, l-1]k_{j,yx}^{\text{inv}})\xi_x V_j \\ & + \frac{\Delta t}{\rho} \gamma_y \sum_{j=1}^{N_i} C(|\xi_{ij}|)(\psi_x[\mathbf{x}_i, l-2]k_{i,xx}^{\text{inv}} + \psi_\tau[\mathbf{x}_i, l-2]k_{i,yx}^{\text{inv}})\xi_x V_j \\ & + \frac{\Delta t}{\rho} \gamma_y \sum_{j=1}^{N_i} C(|\xi_{ij}|)(\psi_x[\mathbf{x}_j, l-2]k_{j,xx}^{\text{inv}} + \psi_\tau[\mathbf{x}_j, l-2]k_{j,yx}^{\text{inv}})\xi_x V_j \\ & + \frac{\Delta t}{\rho} \sum_{j=1}^{N_i} C(|\xi_{ij}|)(\psi_x[\mathbf{x}_i, l-1]k_{i,xy}^{\text{inv}} + \psi_\tau[\mathbf{x}_i, l-1]k_{i,yy}^{\text{inv}})\xi_y V_j \\ & + \frac{\Delta t}{\rho} \sum_{j=1}^{N_i} C(|\xi_{ij}|)(\psi_x[\mathbf{x}_j, l-1]k_{j,xy}^{\text{inv}} + \psi_\tau[\mathbf{x}_j, l-1]k_{j,yy}^{\text{inv}})\xi_y V_j \\ & + \frac{\Delta t}{\rho} \gamma_x \sum_{j=1}^{N_i} C(|\xi_{ij}|)(\psi_x[\mathbf{x}_i, l-2]k_{i,xy}^{\text{inv}} + \psi_\tau[\mathbf{x}_i, l-2]k_{i,yy}^{\text{inv}})\xi_y V_j \\ & + \frac{\Delta t}{\rho} \gamma_x \sum_{j=1}^{N_i} C(|\xi_{ij}|)(\psi_x[\mathbf{x}_j, l-2]k_{j,xy}^{\text{inv}} + \psi_\tau[\mathbf{x}_j, l-2]k_{j,yy}^{\text{inv}})\xi_y V_j, \end{aligned} \quad (2-32)$$

where V_j is the volume of node j , N_i is the number of nodes in the neighborhood of node i , and $\xi_{ij} = \mathbf{x}_j - \mathbf{x}_i$.

3. Results

The PML was tested on two types of problems, first a wave propagation problem, to demonstrate the effectiveness of the PML, and second a crack propagation problem.

3A. Wave propagation. The PML was first tested on a wave propagation problem with PML boundary layers and a Gaussian distribution as an initial condition. Specifically, the x -directed displacement was set to

$$u_x(\mathbf{x}, t = 0) = e^{-200|x - p_{\text{mid}}|^2}, \quad (3-1)$$

where p_{mid} is the midpoint of the region, which in this example was defined as $0 \leq x, y \leq 1$ and discretized with $\Delta x = \Delta y = 0.01$ m. The Young's modulus for the region was set to 1 Pa, the Poisson's ratio was $\frac{1}{4}$, and the density was 1 kg/m^3 . The PML region was defined as the 0.3 m border around the $1 \text{ m} \times 1 \text{ m}$ region and used a Gaussian ramp with a width of 0.2 m, finally reaching a maximum of 50 s^{-1} for the remaining 0.1 m. For the Gaussian kernel, a horizon size of $\delta = 1.1\Delta x$ was used, and for the Heaviside kernel, a horizon of $\delta = 3.1\Delta x$ was used. The kernel constant c in (2-4) and (2-5) is set to 1 throughout.

The simulation was run with both the Heaviside and Gaussian kernels, with the total strain energy shown in Figure 2. The Gaussian kernel (the dotted line) shows the largest drop in energy, reaching a minimum of 5.6×10^{-7} , and the Heaviside kernel (the dashed line) decreases to $1. \times 10^{-4}$. A bounded simulation is shown for reference (the solid line), which used a fixed displacement boundary condition and the Gaussian kernel. Figure 3 shows a waterfall plot of the x -directed displacement along the $y = 0.5$ line for the Gaussian kernel with the PML function ϕ_x shown in gray on the far end of the plot (corresponding to $t = 1$ s). Figure 4 shows the absolute value of the x -directed displacement at the edge of the PML region, in simulations terminated by a PML and with a fixed boundary condition. The wave

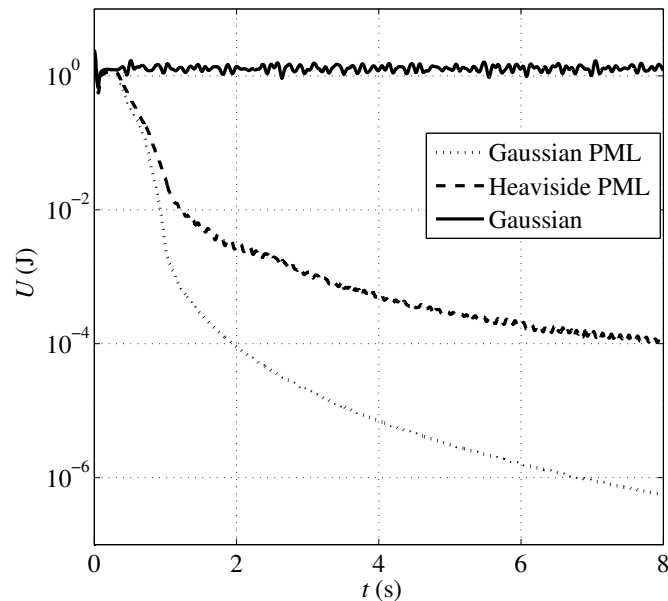


Figure 2. Total strain energy in a simulation terminated by a PML.

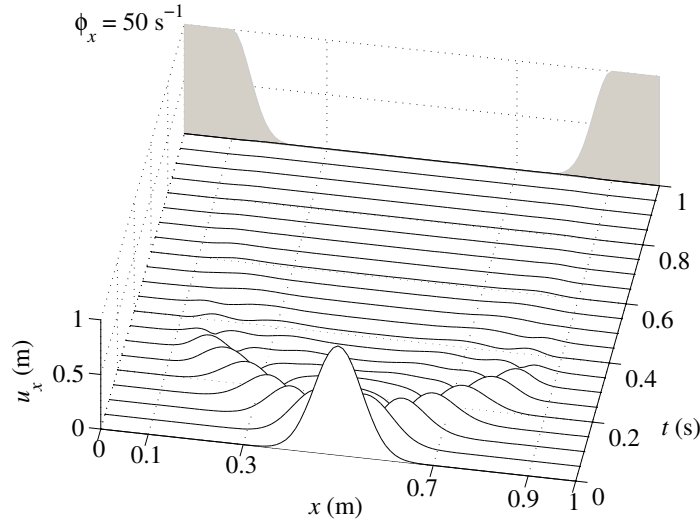


Figure 3. The x -directed displacement at $y = 0.5$ m, terminated by a PML.

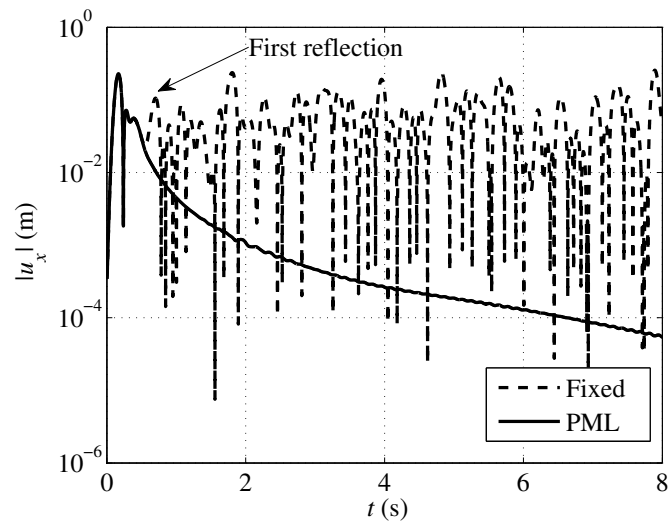


Figure 4. The x -directed displacement at $x = 0.3$, $y = 0.5$ m. The solid line shows results terminated by a PML, and the dashed line used a fixed boundary condition.

is absorbed at the boundary with minimal reflections: as can be seen, the plots align for a time, and where they deviate (indicating a reflection from the hard boundary), the PML simulation remains in decay.

For verification, the method was compared with an exact analytical solution. Consider a cylindrically symmetric wave propagating in an infinite elastic medium with the same constitutive parameters as the above example, and with an initial condition given by

$$u_0(r) = b \left(\frac{r}{a} \right) \left[1 + \left(\frac{r}{a} \right)^2 \right]^{-3/2}, \tag{3-2}$$

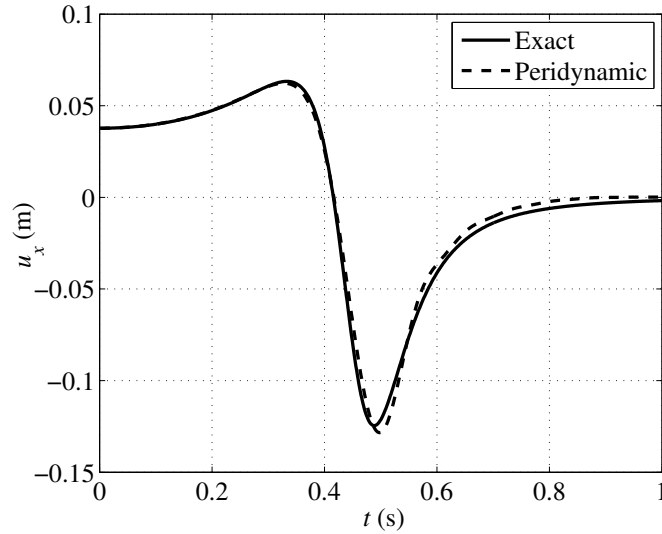


Figure 5. The x -directed displacement at $x = 0.5$, $y = 0$ m. The solid line shows the exact solution and the dashed line results terminated by a PML.

where here we take $b = 1$ and $a = 0.1$. The exact solution is given by [Eringen and Suhubi 1975]

$$u(r, t) = \frac{br}{\sqrt{2a}R^6} \sqrt{R^2 + \alpha(2\alpha - R^2)}, \quad \alpha = 1 + \frac{r^2 - c^2t^2}{a^2}, \quad R^2 = \sqrt{\alpha^2 + \frac{4c^2t^2}{a^2}}, \quad (3-3)$$

where c is the longitudinal wave speed. This problem was simulated in a two-dimensional region, $2 \text{ m} \times 2 \text{ m}$ and $\Delta x = \Delta y = 0.01 \text{ m}$, terminated by a PML with the same dimensions and magnitude as the above problem. The Gaussian kernel was used with a horizon size of $\delta = 0.75\Delta x$, with an actual cutoff of 0.028 m . The results are shown in Figure 5, with the exact solution shown as the solid line and the peridynamic solution shown as the dashed line. The peridynamic solution shows good agreement with the exact solution and minimal reflections from the PML boundary.

3B. Crack propagation. Crack propagation in a half-space can be useful for modeling physical phenomena such as indentation experiments. As an example, we model such a problem as a body force applied to a finite region with small precracks in a region terminated on three sides with PMLs. One addition to the algorithm for this problem was a drag term, used to reduce noise. For crack problems with a sudden force application, noise and oscillations can cause hot spots and undesirable cracking. To remedy this, a drag term can be added to smooth oscillations, by adjusting the nodal velocity as

$$\mathbf{v}^*[\mathbf{x}_i, l] = (1 - D)\mathbf{v}[\mathbf{x}_i, l] + \frac{D}{N_b} \sum_{j=1}^{N_b} \mathbf{v}[\mathbf{x}_j, l], \quad (3-4)$$

where D is the drag coefficient and N_b is the remaining number of bonds in the family of node n [Becker and Lucas 2011].

An absorbing boundary ensures that no reflections from the boundaries interfere with the crack propagation, possibly causing it to deviate. Figure 6 gives a schematic of the problem: the extent of the

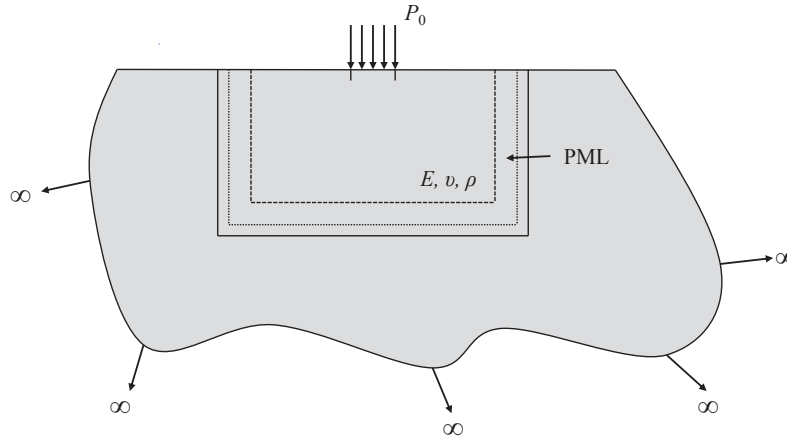


Figure 6. Schematic diagram of the problem for crack propagation in a half-space.

computation region is designated by the solid line, the PML ramp begins at the dashed line, and the PML plateaus at the dotted line. The computational region was 70 mm wide and 35.25 mm high, the PML region began at 15 mm from each edge (except the top) and peaked at 5 mm to a value of $5 \times 10^6 \text{ s}^{-1}$. The node spacing was 0.496 mm and the time step size was 1 ns. For material values, the density was 2235 kg/m^3 , the Young’s modulus was 65 GPa, the Poisson’s ratio was 0.2, and the fracture criteria used a fracture energy of 204 J/m^2 . The failure criteria used in this simulation was bond-based, that is, a bond failed if it was stretched past a given limit, determined by the fracture energy [Ha and Bobaru 2010]. The maximum relative bond stretch was then 2.971×10^{-3} . The load was applied across a 10 mm region, centered at the top surface, with precracks on each edge with a length of two nodes or 0.993 mm. The simulation was run for a total of $10 \mu\text{s}$, and the cracks were measured manually from the edge of the precracks to the extent of the damaged area.

Figure 7 shows a result which had an applied load of 250 N, yielding a 2.11 mm crack. Figure 8 shows a close-up of the damaged area from Figure 7. As can be seen, the crack extends three nodes down and

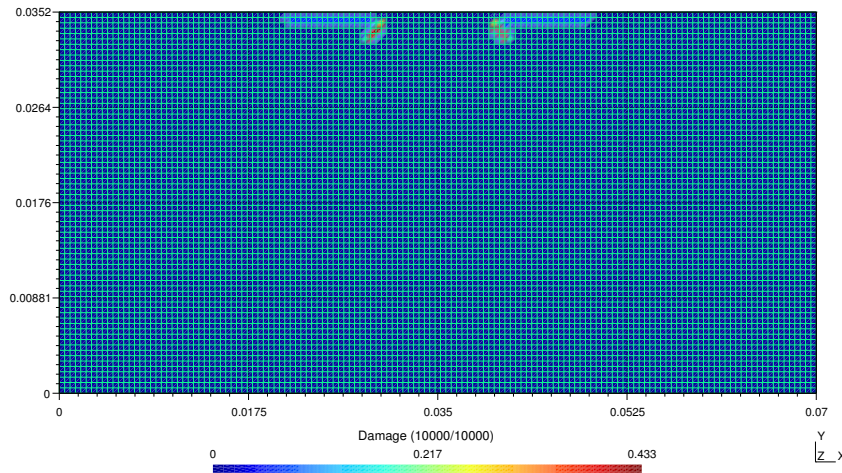


Figure 7. Damage map resulting from a 250 N applied load after $10 \mu\text{s}$.

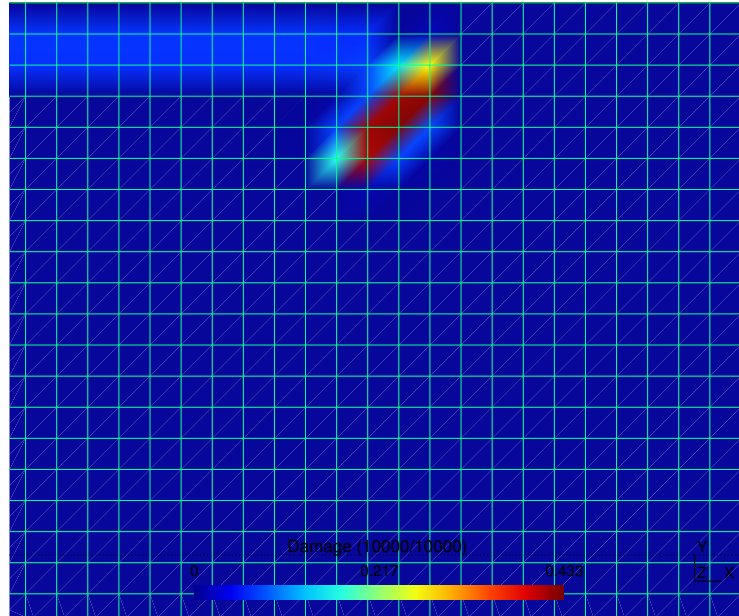


Figure 8. Close-up of damage map from Figure 7.

three nodes across. Finally, the applied load was varied between 140 N and 500 N, with the distance between the crack tips (the crack separation) versus the applied load shown as the dots in Figure 9. A curve, shown as the solid line in Figure 9, was fit using the form

$$d = Ap^s + B, \quad (3-5)$$

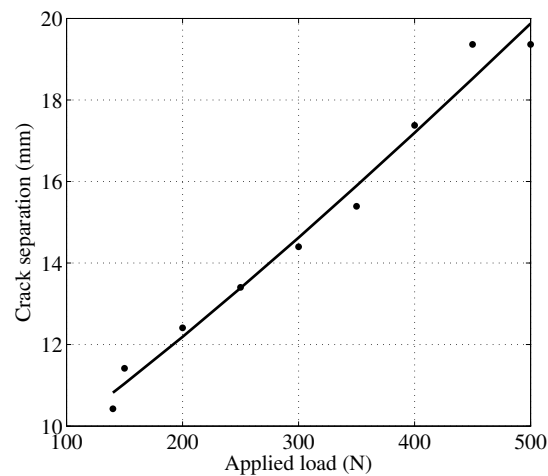


Figure 9. Crack separation versus applied force for indentation into an elastic half-space. Dots represent data points from the peridynamic simulation and the solid line is a curve fit.

where d is the crack tip separation distance, p is the applied load, and $A = 8.49 \times 10^{-3}$ mm/N s , $s = 1.16$ and $B = 8.15$ mm were determined using least squares. The norm of the residual for the curve fit was 1.65×10^{-6} .

4. Conclusions

A perfectly matched layer (PML) was applied to peridynamics in two dimensions, allowing for the simulation of infinite regions. State-based peridynamics was used as more flexible constitutive relations are necessary to implement a perfectly matched layer, essentially an artificial anisotropic absorbing material. Standard discretization techniques were used: one-point integration and point-matching for the spatial discretization and forward Euler for the temporal discretization. Results show that the PML absorbs incoming waves and results in minimal reflections at the boundary between the absorbing layer and the computational region. A Gaussian function was used as a ramp to avoid these numerical reflections. Finally, a crack propagation problem was simulated in a half-space, modeling indentation problems. A three-dimensional implementation of the method would be straightforward, following an identical procedure for the peridynamics and PML formulation.

References

- [Alles and van Dongen 2009] E. J. Alles and K. W. A. van Dongen, "Frequency domain perfectly matched layers for acoustic scattering integral equation problems", pp. 1610–1613 in *2009 IEEE International Ultrasonics Symposium* (Rome, 2009), edited by M. P. Yuhas, IEEE, Piscataway, NJ, 2009.
- [Becker and Lucas 2011] R. Becker and R. J. Lucas, "An assessment of peridynamics for pre and post failure deformation", Technical report ARL-TR-5811, U.S. Army Research Laboratory, Aberdeen, MD, November 2011, Available at <http://www.dtic.mil/cgi-bin/GetTRDoc?AD=ADA553977>.
- [Berenger 1994] J.-P. Berenger, "A perfectly matched layer for the absorption of electromagnetic waves", *J. Comput. Phys.* **114**:2 (1994), 185–200.
- [Bobaru 2007] F. Bobaru, "Influence of van der Waals forces on increasing the strength and toughness in dynamic fracture of nanofibre networks: a peridynamic approach", *Model. Simul. Mater. Sci. Eng.* **15**:5 (2007), 397–417.
- [Bobaru and Duangpanya 2010] F. Bobaru and M. Duangpanya, "The peridynamic formulation for transient heat conduction", *Int. J. Heat Mass Transf.* **53**:19-20 (2010), 4047–4059.
- [Bobaru et al. 2009] F. Bobaru, M. Yang, L. F. Alves, S. A. Silling, E. Askari, and J. Xu, "Convergence, adaptive refinement, and scaling in 1D peridynamics", *Int. J. Numer. Methods Eng.* **77**:6 (2009), 852–877.
- [Chew and Liu 1996] W. C. Chew and Q. H. Liu, "Perfectly matched layers for elastodynamics: a new absorbing boundary condition", *J. Comput. Acoust.* **4**:4 (1996), 341–359.
- [Chew and Weedon 1994] W. C. Chew and W. H. Weedon, "A 3D perfectly matched medium from modified Maxwell's equations with stretched coordinates", *Microw. Opt. Tech. Lett.* **7**:13 (1994), 599–604.
- [Demmie and Silling 2007] P. N. Demmie and S. A. Silling, "An approach to modeling extreme loading of structures using peridynamics", *J. Mech. Mater. Struct.* **2**:10 (2007), 1921–1945.
- [Dong et al. 2004] X. T. Dong, X. S. Rao, Y. B. Gan, B. Guo, and W. Y. Yin, "Perfectly matched layer-absorbing boundary condition for left-handed materials", *IEEE Microw. Wirel. Compon. Lett.* **14**:6 (2004), 301–303.
- [Du et al. 2012] Q. Du, M. D. Gunzburger, R. B. Lehoucq, and K. Zhou, "A nonlocal vector calculus, nonlocal volume-constrained problems, and nonlocal balance laws", *Math. Models Methods Appl. Sci.* (2012). Accepted for publication. Preprint SAND2010-8353J available from Sandia National Laboratories, 2010.
- [Emmrich and Weckner 2006] E. Emmrich and O. Weckner, "The peridynamic model in non-local elasticity theory", *Proc. Appl. Math. Mech.* **6**:1 (2006), 155–156.

- [Emmrich and Weckner 2007] E. Emmrich and O. Weckner, “The peridynamic equation and its spatial discretisation”, *Math. Model. Anal.* **12**:1 (2007), 17–27.
- [Eringen and Suhubi 1975] A. C. Eringen and E. S. Suhubi, *Elastodynamics*, Academic Press, New York, 1975.
- [Festa and Nielsen 2003] G. Festa and S. Nielsen, “PML absorbing boundaries”, *Bull. Seismol. Soc. Am.* **93**:2 (2003), 891–903.
- [Foster et al. 2010] J. T. Foster, S. A. Silling, and W. W. Chen, “Viscoplasticity using peridynamics”, *Int. J. Numer. Methods Eng.* **81**:10 (2010), 1242–1258.
- [Gerstle et al. 2005] W. Gerstle, N. Sau, and S. A. Silling, “Peridynamic modeling of plain and reinforced concrete structures”, pp. 54–88 in *18th International Conference on Structural Mechanics in Reactor Technology* (Beijing, 2005), edited by Y. Zhou, Atomic Energy Press, Beijing, 2005.
- [Gerstle et al. 2008] W. Gerstle, S. A. Silling, D. Read, V. Tewary, and R. Lehoucq, “Peridynamic simulation of electromigration”, *Comput. Mater. Continua* **8**:2 (2008), 75–92.
- [Gerstle et al. 2011] W. Gerstle, N. Sau, and E. Aguilera, “Micropolar peridynamic constitutive model for concrete”, pp. 1–8 in *19th International Conference on Structural Mechanics in Reactor Technology* (Toronto, ON, 2007), edited by V. C. Matzen, Elsevier, Amsterdam, 2011.
- [Ha and Bobaru 2010] Y. D. Ha and F. Bobaru, “Studies of dynamic crack propagation and crack branching with peridynamics”, *Int. J. Fract.* **162**:1-2 (2010), 229–244.
- [Johnson 2010] S. G. Johnson, “Notes on perfectly matched layers”, 2010, Available at <http://math.mit.edu/~stevenj/18.369/pml.pdf>.
- [Kilic et al. 2009] B. Kilic, A. Agwai, and E. Madenci, “Peridynamic theory for progressive damage prediction in center-cracked composite laminates”, *Compos. Struct.* **90**:2 (2009), 141–151.
- [Liu and Tao 1997] Q.-H. Liu and J.-P. Tao, “The perfectly matched layer for acoustic waves in absorptive media”, *J. Acoust. Soc. Am.* **102**:4 (1997), 2072–2082.
- [Lubich 1988a] C. Lubich, “Convolution quadrature and discretized operational calculus, I”, *Numer. Math.* **52**:2 (1988), 129–145.
- [Lubich 1988b] C. Lubich, “Convolution quadrature and discretized operational calculus, II”, *Numer. Math.* **52**:4 (1988), 413–425.
- [Malvern 1969] L. E. Malvern, *Introduction to the mechanics of a continuous medium*, Prentice-Hall, Englewood Cliffs, NJ, 1969.
- [Parks et al. 2008] M. L. Parks, P. Seleson, S. J. Plimpton, R. B. Lehoucq, and S. A. Silling, “Peridynamics with LAMMPS: a user guide”, Technical report SAND2008-0135, Sandia National Laboratories, Albuquerque, NM, July 2008. Superseded by SAND2010-5549, version 0.2 Beta, August 2010.
- [Pissoort and Olyslager 2003] D. Pissort and F. Olyslager, “Termination of periodic waveguides by PMLs in time-harmonic integral equation-like techniques”, *IEEE Antenn. Wirel. Propag. Lett.* **2**:20 (2003), 281–284.
- [Pissoort et al. 2005] D. Pissort, D. Vande Ginste, and F. Olyslager, “Including PML-based absorbing boundary conditions in the MLFMA”, *IEEE Antenn. Wirel. Propag. Lett.* **4**:1 (2005), 312–315.
- [Proakis and Manolakis 1996] J. G. Proakis and D. G. Manolakis, *Digital signal processing: principles, algorithms, and applications*, Prentice-Hall, Upper Saddle River, NJ, 1996.
- [Silling 2000] S. A. Silling, “Reformulation of elasticity theory for discontinuities and long-range forces”, *J. Mech. Phys. Solids* **48**:1 (2000), 175–209.
- [Silling and Askari 2005] S. A. Silling and E. Askari, “A meshfree method based on the peridynamic model of solid mechanics”, *Comput. Struct.* **83**:17-18 (2005), 1526–1535.
- [Silling et al. 2007] S. A. Silling, M. Epton, O. Weckner, J. Xu, and E. Askari, “Peridynamic states and constitutive modeling”, *J. Elasticity* **88**:2 (2007), 151–184.
- [Teixeira and Chew 1998] F. L. Teixeira and W. C. Chew, “A general approach to extend Berenger’s absorbing boundary condition to anisotropic and dispersive media”, *IEEE Trans. Antenn. Propag.* **46**:9 (1998), 1386–1387.
- [Uno et al. 1997] T. Uno, Y. He, and S. Adachi, “Perfectly matched layer absorbing boundary condition for dispersive medium”, *IEEE Microw. Guided Wave Lett.* **7**:9 (1997), 264–266.

- [Wang et al. 2008] X. Wang, R. A. Wildman, D. S. Weile, and P. Monk, “A finite difference delay modeling approach to the discretization of the time domain integral equations of electromagnetics”, *IEEE Trans. Antenn. Propag.* **56**:8, part 1 (2008), 2442–2452.
- [Weckner and Abeyaratne 2005] O. Weckner and R. Abeyaratne, “The effect of long-range forces on the dynamics of a bar”, *J. Mech. Phys. Solids* **53**:3 (2005), 705–728.
- [Weckner et al. 2009] O. Weckner, G. Brunk, M. A. Epton, S. A. Silling, and E. Askari, “Green’s functions in non-local three-dimensional linear elasticity”, *Proc. R. Soc. Lond. A* **465**:2111 (2009), 3463–3487.
- [Wildman and Gazonas 2011] R. A. Wildman and G. A. Gazonas, “A perfectly matched layer for peridynamics in one dimension”, Technical report ARL-TR-5626, U.S. Army Research Laboratory, Aberdeen, MD, 2011.

Received 2 Apr 2012. Revised 17 Jul 2012. Accepted 18 Jul 2012.

RAYMOND A. WILDMAN: raymond.a.wildman.civ@mail.mil

*Weapons and Materials Research Directorate, U.S. Army Research Laboratory, Attn: RDRL-WMM-B,
Aberdeen Proving Ground, MD 21005, United States*

GEORGE A. GAZONAS: george.a.gazonas.civ@mail.mil

*Weapons and Materials Research Directorate, U.S. Army Research Laboratory, ATTN: RDRL-WMM-B,
Aberdeen Proving Ground, MD 21005, United States*

JOURNAL OF MECHANICS OF MATERIALS AND STRUCTURES

jomms.net

Founded by Charles R. Steele and Marie-Louise Steele

EDITORS

CHARLES R. STEELE Stanford University, USA
DAVIDE BIGONI University of Trento, Italy
IWONA JASIUK University of Illinois at Urbana-Champaign, USA
YASUhide SHINDO Tohoku University, Japan

EDITORIAL BOARD

H. D. BUI École Polytechnique, France
J. P. CARTER University of Sydney, Australia
R. M. CHRISTENSEN Stanford University, USA
G. M. L. GLADWELL University of Waterloo, Canada
D. H. HODGES Georgia Institute of Technology, USA
J. HUTCHINSON Harvard University, USA
C. HWU National Cheng Kung University, Taiwan
B. L. KARIHALOO University of Wales, UK
Y. Y. KIM Seoul National University, Republic of Korea
Z. MROZ Academy of Science, Poland
D. PAMPLONA Universidade Católica do Rio de Janeiro, Brazil
M. B. RUBIN Technion, Haifa, Israel
A. N. SHUPIKOV Ukrainian Academy of Sciences, Ukraine
T. TARNAI University Budapest, Hungary
F. Y. M. WAN University of California, Irvine, USA
P. WRIGGERS Universität Hannover, Germany
W. YANG Tsinghua University, China
F. ZIEGLER Technische Universität Wien, Austria

PRODUCTION production@msp.org

SILVIO LEVY Scientific Editor

Cover design: Alex Scorpan

See <http://jomms.net> for submission guidelines.

JoMMS (ISSN 1559-3959) is published in 10 issues a year. The subscription price for 2012 is US \$555/year for the electronic version, and \$735/year (+\$60 shipping outside the US) for print and electronic. Subscriptions, requests for back issues, and changes of address should be sent to Mathematical Sciences Publishers, Department of Mathematics, University of California, Berkeley, CA 94720-3840.

JoMMS peer-review and production is managed by EditFLOW[®] from Mathematical Sciences Publishers.

PUBLISHED BY
 **mathematical sciences publishers**
<http://msp.org/>

A NON-PROFIT CORPORATION

Typeset in L^AT_EX

Copyright ©2012 by Mathematical Sciences Publishers

Journal of Mechanics of Materials and Structures

Volume 7, No. 8-9

October 2012

A model for the shear displacement distribution of a flow line in the adiabatic shear band based on gradient-dependent plasticity

XUE-BIN WANG and BING MA 735

A pull-out model for perfectly bonded carbon nanotube in polymer composites

KHONDAKER SAKIL AHMED and ANG KOK KENG 753

A perfectly matched layer for peridynamics in two dimensions

RAYMOND A. WILDMAN and GEORGE A. GAZONAS 765

Displacement field in an elastic solid with mode-III crack and first-order surface effects

TAMRAN H. LENGYEL and PETER SCHIAVONE 783

On the choice of functions spaces in the limit analysis for masonry bodies

MASSIMILIANO LUCCHESI, MIROSLAV ŠILHAVÝ and NICOLA ZANI 795

Edge stiffness effects on thin-film laminated double glazing system dynamical behavior by the operational modal analysis

ALI AKROUT, MARIEM MILADI CHAABANE, LOTFI HAMMAMI and MOHAMED HADDAR 837

Network evolution model of anisotropic stress softening in filled rubber-like materials

ROOZBEH DARGAZANY, VU NGOC KHIÊM, UWE NAVRATH and MIKHAIL ITSKOV 861



1559-3959(2012)7:8;1-6